High solar flux concentration water splitting with hematite (α-Fe₂O₃) photoanodes

Gideon Segev,[1] *Hen Dotan,*[1] *Kirtiman Deo Malviya,*[1] *Asaf Kay,*[1] *Matthew T. Mayer,*[2] *Michael Grätzel*[2] *and Avner Rothschild* [1,*]

[1] Department of Materials Science and Engineering, Technion- Israel Institute of Technology, Haifa, Israel, 3200003, Israel
[2] Institute of Chemical Sciences and Engineering, Ecole Polytechnique Federale de Lausanne, 1015 Lausanne, Switzerland
*E-mail: avner@mt.technion.ac.il

Hematite (α-Fe₂O₃) photoanodes are widely studied as candidates for water splitting photoelectrochemical cells. Despite considerable progress in the design of hematite photoanodes, their power conversion efficiency is still quite low and there is much room for further improvement in the photocurrent and photovoltage. This work examines the performance of hematite photoanodes under high solar-simulated flux concentrations, exploring another route for efficiency enhancement. Unlike concentrated photovoltaics (CPV), very little is known on the performance of water splitting photoelectrochemical cells and hematite photoanodes under high illumination intensities. We find that the photocurrent density scales linearly with the flux concentration, as in CPV, whereas the photovoltage scales logarithmically with the flux concentration at a considerably faster rate than in CPV. These observations demonstrate the potential of flux concertation as a means to enhance the performance of hematite photoanodes for water splitting tandem cells, and they shed new light on the water photo-oxidation mechanism.

The need for cost effective and sustainable technologies for storing intermittent solar power spurs a growing interest in artificial photosynthesis and solar fuels.[1,2] Photoelectrochemical (PEC) cells combined in tandem with photovoltaic (PV) cells offer a

viable solution to this need by splitting water, using solar power, to hydrogen and oxygen.[3,4] The hydrogen can be stored and converted to electricity on-demand (e.g., by fuel cells), or be used as renewable feedstock for sustainable synthesis of liquid fuels (e.g., by hydrogenation of CO_2).[5,6] One of the greatest challenges in this route is the development of stable, efficient and inexpensive photoanodes for water photo-oxidation. Hematite (α-Fe_2O_3) is a leading photoanode candidate[7–11] due to its abundance, stability in alkaline aqueous solutions, high catalytic activity for water oxidation[12] and bandgap energy of 2.1 eV which is nearly optimal for tandem cells in combination with lower bandgap semiconductors such as Si.[13] However, hematite also displays deleterious charge transport properties that complicate the development of high efficiency photoanodes. First, it has poor charge carrier mobility[14] and therefore hematite photoanodes are usually heavily doped by donors such as Si or Ti (typically ~1-2 at.%) in order to reduce their internal resistance.[7] Second, hematite has short lifetime of excess charge carriers[15] that gives rise to deleterious recombination, which is further enhanced by high doping density.[16] As a result, the diffusion length of excess charge carriers is extremely small,[17] and therefore effective collection of photo-generated charge carriers is confined, for the most part, to the depletion region adjacent to the surface,[18] which is quite small because of the high doping density. The width of the depletion region increases with anodic bias, as in semiconductor junctions under reverse bias,[19] and high pH, thereby enhancing the collection efficiency of photo-generated charge carriers and, consequently, the water photo-oxidation current density.[18,20,21] On top of bulk recombination that reduces the flux of photo-generated holes to the surface, holes that have reached the surface, so-called 'long-lived holes',[22–24] may recombine with electrons, giving rise to deleterious back recombination that competes with the forward charge transfer reaction, i.e., water oxidation.[21,25,26] In order to suppress the back recombination high anodic bias is applied to reduce the electron concentration at the surface and in the depletion region.[21,25,26] But this comes with a toll that shows up as excess anodic bias that is applied in order to suppress

2

recombination of photo-generated charge carriers, both in the bulk and at the surface. Thus, recombination of excess charge carriers is the root cause for the late onset of water photo-oxidation in hematite photoanodes, which requires high anodic bias in order to drive the photocurrent.

High anodic bias diminishes the electrolysis efficiency, and therefore different strategies have been scrutinized in order to reduce this toll, aiming to achieve large photocurrents (the theoretical limit for hematite is 12.6 mA/cm^2 at AM1.5G insolation)[7] at low anodic bias (the ultimate limit is the flat-band potential, which is typically 0.4 - 0.6 V$_{RHE}$, that is volts against the reversible hydrogen electrode, for heavily doped hematite photoanodes in alkaline aqueous solutions).[7] Among the most successful strategies, resonant light trapping in ultrathin (~20-30 nm) compact (i.e., nonporous) films[27] or nanostructuring of thicker (~400-500 nm) mesoporous layers[28,29] were found to enhance the charge collection efficiency by confining the absorbed light close to the surface, thereby reducing bulk recombination. Underlayers were found to enhance charge separation and suppress recombination at the interface with the current collector.[27,30] Surface treatments and overlayers were found to reduce surface recombination and enhance the photovoltage of hematite photoanodes.[31–33] These strategies have yielded considerable improvement in the performance of hematite photoanodes, but despite the progress the performance still remains far below the theoretical limit and is currently too low for technological implementation in PEC cells for solar water splitting. Therefore, new approaches that could possibly lead to further improvement in performance beyond or on top of the existing ones are being sought-after.

This work explores solar flux concentration as a possible means to improve the performance of hematite photoanodes by enhancing the photocurrent and/or reducing the applied bias. The inspiration comes from concentrated photovoltaics (CPV) wherein the power conversion efficiency (PCE) is known to increase at high flux concentrations, as long

as spurious heating and series resistance losses are properly diminished. Moreover, high injection levels are known to increase the lifetime of excess charge carriers in heavily doped semiconductors,[16] which seems to be the bottleneck impeding the development of high efficiency hematite photoanodes. Unlike CPV cells that have been studied extensively in a wide range of flux concentrations, there is little known on the effect of flux concentration on the performance of PEC cells for water splitting, especially hematite photoanodes. In one of the landmark studies on PEC water splitting at high flux concentrations, Khaselev and Turner reported measurements of a p-GaInP$_2$/GaAs tandem cell that were carried out under concentrated illumination form a tungsten-halogen lamp at radiation power density equivalent to 12 Suns.[34] However, the p-type GaInP$_2$ photocathode was unstable and the effects of flux concentration on the photocurrent and photovoltage were not elaborated. Subsequently, Wang et al. studied the performance of p-type GaInP$_2$ photocathodes coupled in tandem with hematite or WO$_3$ photoanodes and measured under light intensities of up to 10 Suns.[35] However, both the hematite and WO$_3$ photoanodes in this work displayed much smaller photocurrents with respect to state-of-the-art photoanodes, making it difficult to assess the relevance for high efficiency photoanodes. Moreover, Reference [35] reports the performance of the entire tandem cell, making it difficult to evaluate the effect of flux concentration on the intrinsic properties of the photoanode. Pioneering work on the performance of a regenerative hematite PEC cells was done by Klahr and Hamann under flux concentrations ranging from 0.35 to 3.9.[36] However, it is difficult to extrapolate from this work to non-regenerative water splitting cells, as we shall see in the following.

Besides the effect on performance, the light intensity also serves as a control parameter that can be tuned in order to investigate the water photoelectrolysis mechanism. Indeed, considerable work was done debating the existence of light intensity threshold for the water photoelectrolysis reaction.[37–40] However, these studies focused, naturally, on low light intensities rather than high solar flux concentrations, and the photoanodes were made of TiO$_2$

and SrTiO$_3$ whose water photo-oxidation mechanism is quite different, most likely, from that of hematite. More recently, Peter et al.[41] and Durrant et al.[26] explored the use of light intensity as a control parameter to investigate the charge carrier dynamics underlying water photo-oxidation by hematite photoanodes. The radiation power in these studies was below 1 Sun (100 mW/cm^2), for the most part. Peter et al. found that the competition between charge transfer and recombination rates leans more toward charge transfer with increasing light intensity,[41] and Durrant et al. found that the lifetime of 'long-lived holes' increases with increasing light intensity.[26] These encouraging observations suggest that high flux concentration might be beneficial for hematite photoanodes.

In this work we explore the water photo-oxidation performance of hematite photoanodes under a wide range of solar-simulated flux concentrations. The effect of flux concentration on the photocurrent and photovoltage is extracted from three-electrode voltammetry measurements in the dark and under illumination, at different flux concentrations, using the methodology that was reported recently in Reference [42]. This enables analyzing the intrinsic PV characteristics of the photoanode as a function of the flux concentration, and comparing them to conventional CPV cells. The photocurrent density at the maximum power point is found to scale linearly with the flux concentration, as expected, whereas the photovoltage scales logarithmically with the flux concentration at a steeper rate than expected. Thus, the anodic potential at the maximum power point decreases and the PCE increases with increasing flux concentrations, demonstrating the advantage of high solar flux concentration water splitting.

The water photo-oxidation characteristics of two different kinds of hematite photoanodes, a compact (nonporous) thin film (50 nm) Ti-doped hematite photoanode and a mesoporous thick layer (500 nm) Si-doped hematite photoanode, were studied by three-electrode voltammetry measurements in 1M NaOH aqueous solution under solar-simulated flux concentrations ranging from ~0.5 to ~25 Suns. The compact thin film photoanode

(sample A) was prepared by pulsed laser deposition (PLD) from a 1 cation% Ti-doped Fe_2O_3

target (see supporting information, Figure S1) onto an FTO-coated glass substrate (TEC15,

Pilkington). Although this photoanode does not achieve the highest photocurrent reported for

thin film hematite photoanodes,[27] it is a convenient, stable and reproducible photoanode

serving as a gold standard for exploring new ideas.[43] It has a typical polycrystalline thin film

morphology and a thickness of 50 nm (see supporting information, Figures S2 – S6). Further

details on the fabrication method of sample A, its microstructural characteristics and PEC

properties (under 1 Sun illumination) can be found elsewhere.[43] The mesoporous thick layer

photoanode (sample B) was prepared by atmospheric pressure chemical vapor deposition

(APCVD) onto an FTO-coated glass substrate following the recipe that produced champion

hematite photoanodes.[28] It has cauliflower morphology (see supporting information, Figure

S7) and a film thickness of ~500 nm. Further details on the fabrication method of sample B,

its microstructural characteristics and PEC properties (under 1 Sun illumination) are reported

elsewhere.[28,33] The PEC measurements followed standard procedures that we use

routinely,[43] except for the flux concentration. Careful attention was given to ensure

reproducible results at different flux concentrations, avoiding possible artifacts such as

spurious heating and different spectral characteristics of the optical system at different flux

concentrations. **Figure 1** shows an example of chopped-light voltammetry measurements

obtained with sample A at a flux concentration of 5.4. The left axis shows the current in mA

(the illuminated area of the photoanode was 0.28 cm^2) and the right axis shows the

corresponding applied potential, U_{app}, in volts against the reversible hydrogen electrode

(RHE). The inset shows magnification of the measured current between 445 and 490 s. The

current values for the construction of the current density vs. applied potential curves in **Figure**

2(a) are the mean current values between $0.5T_{on}$ and $0.9T_{on}$ where T_{on} is the illumination

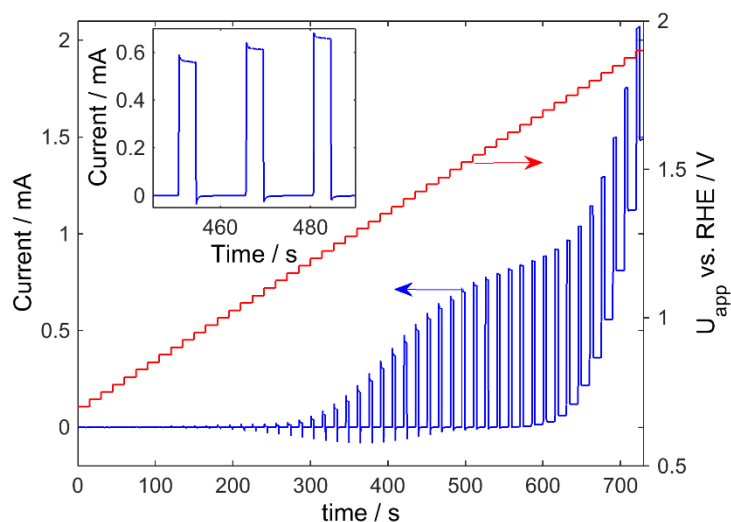period within each cycle. The same measurement procedure was carried out with sample B.

Figure 1. Chopped-light voltammetry measurements of sample A at a solar-simulated flux concentration of 5.4.

For sample A, voltammetry measurements were taken at solar-simulated flux concentrations ranging from 0.57 to 27.2 Suns. At first, the flux concentration was increased from one voltammetry scan to another by several steps until reaching the maximum flux concentration (27.2 Suns). Next, in order to examine repeatability, the measurements where repeated in the reverse direction, decreasing the flux concentration from the maximum (27.2 Suns) until reaching a minimum of 0.57. In order to diminish spurious heating at high flux concentrations of 3.6 or higher ($X \geq 3.6$), chopped light measurements were carried out with a duty cycle of 20%. At lower flux concentrations linear sweep voltammetry measurements were carried out without chopping the light. Figures 2(a) shows the current density vs. applied potential curves obtained for samples A at various flux concentrations. Solid lines represent voltammograms obtained while increasing the flux concentration from 1 (blue curve) to 3.6 (pale blue curve). Circles represent chopped-light voltammetry measurements obtained while increasing the flux concentration from 3.6 (pale blue circles) to 27.2 (dark red circles). Squares represent chopped light voltammetry measurements taken while decreasing the flux concentration to 21 (red squares) and then to 11 (yellow squares). Dashed lines represent voltammograms

7

measured while decreasing the flux concentration from 3.6 (pale blue curve) to 0.57 (blue

curve). One can see that the results are repeatable, displaying negligible difference between

the first set of measurements and the second one. Similar measurements were carried out with

sample B, at flux concentrations ranging from 0.48 to 25.6, wherein chopped light

measurements were carried out at flux concentrations of 2.6 or higher ($X \geq 2.6$). Figures 2(b)

shows the current density vs. applied potential curves obtained at various flux concentrations

for sample B. Solid lines represent voltammograms obtained while increasing the flux

concentration from 0.48 (blue curve) to 2.6 (pale blue curve). Circles represent chopped light

voltammetry measurements obtained while increasing the flux concentration from 2.6 (pale

blue circles) to 25.6 (dark red circles). Both samples, A and B, displayed similar effect of flux

concentration on the photocurrent, despite the fact that sample B reached much higher
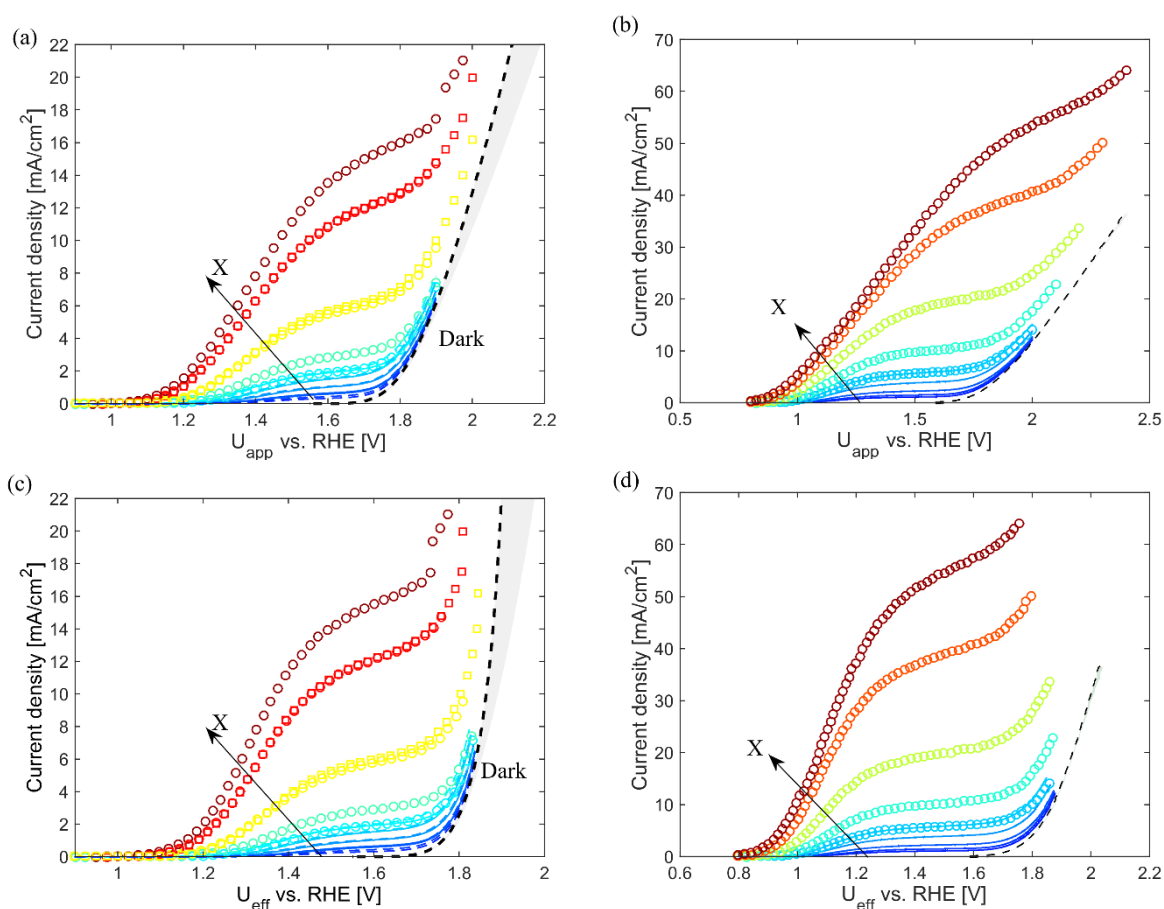
photocurrents than sample A.

Figure 2. Current density vs. applied potential curves measured at various flux concentrations with sample A (a) and B (b), and compensated curves for samples A (c) and B (d) showing the current density vs. effective potential wherein the effect of uncompensated series resistance was removed according to equation (1). For sample A the flux concentration was varied between $X = 0.57$ (dashed blue curve) and 27.2 (dark red circles), whereas for sample B the flux concentration was varied between $X = 0.48$ (dashed blue curve) and 25.6 (dark red circles).

The black dashed curves in Figures 2(a) and (b) show the dark currents of the respective measurements. For sample A we observed small variations in the dark current from one measurement and another (see supporting information, Figure S12(a)). In the analysis that follows we took the dark current values that were obtained in the last measurement, which were slightly larger than in previous ones, probably due to some aging effect.[44] This is a conservative analysis and the error induced by the small variations in the dark current values is discussed in the supporting information. For sample B the dark current shows excellent repeatability with negligible variations between different measurements (see supporting information, Figure S12(b)). At current densities above 30 mA/cm^2 the measurements were disturbed by bubbles. This was less of an issue in the chopped-light measurements wherein the bubbles were removed in the dark periods between the illumination cycles. As can be seen in Figures 2(a) and (b), the dark current displays a sloped linear curve at high current values. This is indicative of uncompensated series resistance loss that arise, most likely, from the resistance of the FTO current collector.[45] To compensate for this artifact the raw data were corrected by computing the actual effective potential at the working electrode, U_{eff}: [46]

$$U_{eff} = U_{app} - I \cdot R_s \tag{1}$$

where I is the measured current, U_{app} is the applied potential, and $R_s = 34.4 \pm 0.3$ Ω for sample A or 36 ± 1 Ω for sample B is the uncompensated series resistance, as obtained from electrochemical impedance spectroscopy measurements (see supporting information, Figure S13).[46] Figures 2(c) and (d) present the compensated curves of samples A and B, respectively, showing the current density vs. effective potential as obtained from the raw data

in Figures 2(a) and (b), respectively, with the potential correction as per equation (1). From here on we consider only the compensated curves, Figures 2(c) and (d), rather than the measured ones, Figures 2(a) and (b).

In order to gain better understanding of the performance of the photoanodes, their intrinsic photovoltaic characteristics, that is the photocurrent density, J_{photo}, and photovoltage, V_{photo}, where extracted from the current density vs. effective potential compensated curves in Figures 2(c) and (d) using the procedure described in Reference [42]. For sample A, the reference is made to the highest dark current values (represented by the dashed black curve in Figure 2(c)). Hence the extracted V_{photo} values give conservative estimation of the lower bound of the actual photovoltage values. For sample B the dark current variations were negligible, therefore the inaccuracy in the V_{photo} values extracted from Figure 2(d) is negligibly small. Complementary measurements were carried out for sample A in the presence of hole scavenger (H_2O_2)[20] in the 1M NaOH aqueous electrolyte solution, yielding large dark currents at smaller potentials than the onset of water oxidation in the dark (see supporting information, Figure S14). This shows that no rectification overpotential losses[47] prevailed during water oxidation. Thus, the prerequisite for the photovoltage extraction from the voltammograms obtained in the dark and under illumination, that is that the internal resistance of the working electrode is negligible (or else it must be properly compensated for),[42] is fulfilled, since the remaining internal resistance ($I·R$) loss due to the series resistance of the working electrode is already compensated for by equation (1). Therefore, the analysis is valid since the possible contributions to the internal resistance loss are either absent (rectification) or properly compensated for (series resistance).

Figures 3(a) and (b) show the photocurrent density as a function of the calculated photovoltage for different flux concentrations, as derived from the data presented in Figures 2(c) and (d), respectively. For sample B, the analysis was carried out up to a flux concentration of 16.7. At higher flux concentrations the results were too noisy because of

massive bubble formation at high currents. Similarly to the photocurrent of photovoltaic cells, the plateau photocurrent increases with increasing flux concentrations. The insets in Figure 3 show the photocurrent density normalized by the flux concentration, X, as a function of the photovoltage. As can be seen in the insets, the normalized plateau photocurrent is nearly constant, independent of the flux concentration. This observation confirms the expected linear relation between the plateau photocurrent and the flux concentration, in agreement with the results reported recently by Durrant et al. for hematite photoanodes measured in flux concentrations ranging from 0.16 to 1.29 Suns.[26] Despite the fact that sample B greatly outperforms sample A in terms of both the photocurrent, photovoltage and fill factor, the photovoltaic characteristics of both samples show similar trends with respect to the effect of flux concentration. It is noteworthy that the fill factor of sample B increases with the flux concentration more prominently than in sample A. This leads to stronger enhancement of the photovoltage at the maximum power point, $V_{photo,mpp}$, at high flux concentrations in sample B than in sample A, as we shall see in the following.
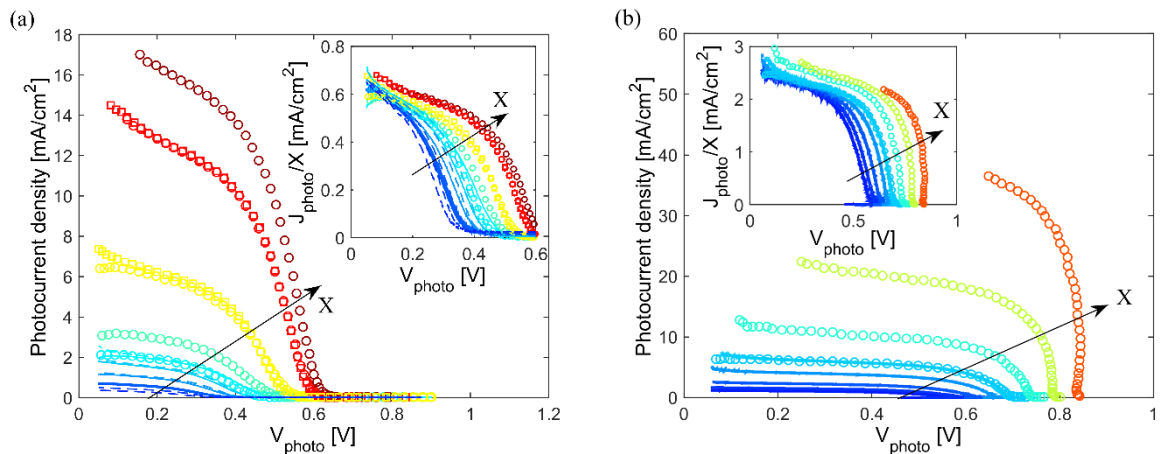

Figure 3. The photocurrent density as a function of the calculated photovoltage for various flux concentrations obtained for samples A (a) and B (b). The insets show the photocurrent density normalized by the flux concentration, X, as a function of the calculated photovoltage. The symbol and color codes are the same as in Figure. 2.

The maximum power points wherein the $J_{photo} \times V_{photo}$ product is maximal were extracted from the curves in Figure 3, as widely done in photovoltaics and as discussed in Reference [42]. **Figure 4** shows the photocurrent density at the maximum power point, $J_{photo,mpp}$, as a function of the flux concentration. The dashed black curves represents the best linear fit. For sample A, $J_{photo,mpp} = (0.474 \pm 0.006) \cdot X + (-0.08 \pm 0.06)$ mA/cm^2, and for sample B, $J_{photo,mpp} = (2.073 \pm 0.04) \cdot X + (-0.2 \pm 0.26)$ mA/cm^2, both with R^2 = 0.999. The linear dependence of $J_{photo,mpp}$ on the flux concentration resembles that of CPV cells in the absence of series resistance loss. The different slopes between samples A and B represent the difference in their photocurrent measured in standard 1 Sun illumination conditions.
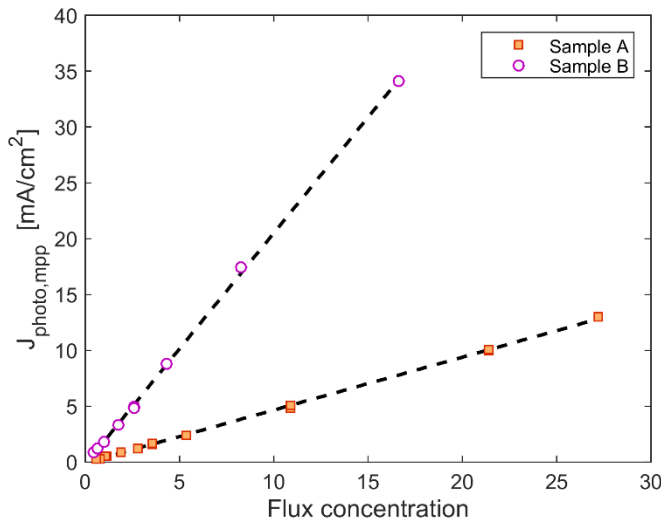

Figure 4. Photocurrent density at the maximum power point as a function of the flux concentration.

As can be seen in the inset of Figure 3, the normalized J_{photo} / X vs. V_{photo} curves shift to higher photovoltages with increasing flux concentrations. This shows that the photovoltage increases with increasing flux concentrations. As a result, the maximum power points shift to higher photovoltages with increasing flux concentrations. **Figures 5(a)** and (b) show the photovoltage at the maximum power points, $V_{photo,mpp}$, as a function of the flux concentration (orange squares) for samples A and B, respectively. In addition, the photo-induced shift in the onset potential, ΔV_{onset}, is also shown by the blue circles. Both $V_{photo,mpp}$ and ΔV_{onset} display

12

logarithmic dependence on the flux concentration, with slopes of 135 and 211 mV per decade, respectively, for sample A, and 188 and 152 mV per decade, respectively, for sample B. In sample B, $V_{photo,mpp}$ increases with the flux concentration faster than ΔV_{onset} because of the enhancement in the fill factor at high flux concertation (see Figure 3(b)). These results show the advantage of flux concentration as a means to enhance the PCE; the photocurrent scales linearly with the flux concentration, $J_{photo} \propto X$, as shown in Figure 4, and on top of that the photovoltage scales logarithmically with the flux concentration, $V_{photo} \propto \log(X)$, as shown in Figure 5. Thus, the PCE, which scales with $J_{photo} \times V_{photo} / P_{in}$,[42] increases logarithmically with increasing flux concentrations because the incident solar power, P_{in}, scales linearly with the flux concentration, $P_{in} \propto X$, similarly to the photocurrent. Therefore, the photovoltage dependence on the flux concentration results in overall PCE enhancement.
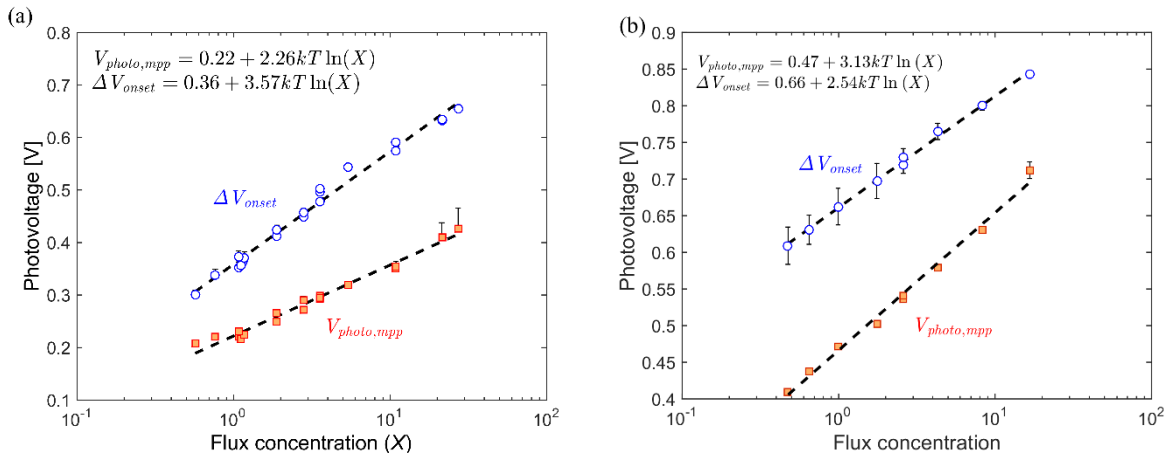

Figure 5. The photovoltage at the maximum power point (orange squares) and the photo-induced shift in the onset potential (blue circles) as a function of the flux concentration for samples A (a) and B (b).

The photo-induced shift in the onset potential, ΔV_{onset}, shown by the blue circles in Figure 5, was found to increase with the flux concentration by 211 mV per decade for sample A and 152 mv per decade for sample B. This is considerably steeper than the rate of increase in the open-circuit voltage of CPV cells, reported to be 57, 60 and 76 mV per decade of flux concentration in state-of-the-art Si, GaAs and CIGS CPV cells, respectively.[48–50] Moreover,

it is much steeper than the rate of increase in the open-circuit voltage of hematite-based regenerative PEC cells, which can be readily extracted from the results reported by Klahr and Hamann in reference [36]. This implies a non-trivial effect that gives rise to steeper slope (i.e., stronger effect) than expected. The root cause underlying this non-trivial effect is unlikely to be an artifact arising from spurious heating, because the maximum temperature rise during measurements at the highest flux concentration was found to be less than 10°C (see supporting information, Figure S11). Therefore, it is, most probably, a real effect that can be utilized to improve the performance of hematite photoanodes.

The non-trivial effect that gives rise to the steep slopes in Figure 5, steeper than in state-of-the-art CPV cells[48–50] as well as hematite-based regenerative PEC cells,[36] is consistent with recent reports on the effect of light intensity on the charge carrier dynamics underlying the water photo-oxidation reaction in hematite photoanodes.[26,41] The latter gives rise to more favorable ratio between charge transfer and recombination rates and longer lifetime of 'long-lived holes' with increasing light intensity, as reported by Peter et al.[41] and by Durrant et al.[26], respectively. Indeed, complementary voltammetry measurements with hole scavenger (H_2O_2) in the electrolyte solution (1M NaOH) carried out with sample A (see supporting information, Figure S15) show that the charge transfer efficiency, obtained from the ratio between the photocurrent measured without the hole scavenger and the photocurrent measured with the hole scavenger,[20] shifts to lower potentials with increasing flux concentration (see supporting information, Figure S16). In contrast, the charge separation and collection efficiency, which scales with the photocurrent measured with the hole scavenger normalized by the flux concentration,[20] is independent of the flux concentration (see supporting information, inset in Figure S16). This observation confirms that high flux concentrations enhance the charge transfer kinetics. We hypothesize that the root cause underlying these observations could possibly arise from saturation of recombination centers, probably at the surface, at high injection levels.[16] Further empirical and theoretical work is

14

undergoing in our lab to examine this hypothesis, but nonetheless the empirical observations stand by their own, whether the hypothesis is right or wrong.

In summary, we found that the water photo-oxidation current density of two different kinds of hematite photoanodes with markedly different thickness (50 and 500 nm), morphology (polycrystalline dense film and mesoporous layer with cauliflower structure), and dopants (Ti and Si) scales linearly with the solar-simulated light intensity at flux concentrations ranging from below 1 to above 25 Suns. The photovoltage was found to scale logarithmically with the flux concentration, with a considerably steeper slope than in CPV cells. These empirical observations are very encouraging, demonstrating another route to improve the efficiency of hematite photoanodes that could possibly be superimposed on top of other optimization strategies such as light trapping, nanostructuring, surface treatment and underlayer and overlayer sensitization schemes. They are consistent with recent reports from other research groups on the effect of light intensity on the charge carrier dynamics underlying the water photo-oxidation reaction on hematite photoanodes. Further research is undergoing in our lab aiming to elucidate the root cause and understand the physics underlying the non-trivial effect that gives rise to the steep dependence of the photovoltage on the flux concentration.

Experimental Section

Sample A comprises a thin (50 nm) film of Ti-doped hematite (α-Fe_2O_3) deposited by pulsed laser deposition (PLD) from a 1 cation% Ti-doped Fe_2O_3 target onto a cleaned FTO-coated glass substrate (Pilkington's TEC15). The deposition was carried out using 9000 laser pulses at a set-point temperature of 500°C in a 25 mTorr O_2 atmosphere. Further details on the fabrication and characterization of this photoanode are given in the supporting information and elsewhere.[43] Sample B was prepared by atmospheric pressure chemical vapor deposition

15

(APCVD) of Si-doped hematite onto a cleaned FTO-coated glass substrate heated atop a heating stage set at 545°C. Iron pentacarbonyl (Fe(CO)$_5$, 99.5%, Acros) and tetraethoxysilane (TEOS, 99.999%, Aldrich) were used as precursors for Fe and Si, respectively. First, a 90 s dose of TEOS vapor was delivered to the heated substrate, followed by a 90 s dose of combined Fe(CO)$_5$ and TEOS vapor, each at a controlled flow rate in air as a carrier gas. After resting 90 s more on the heater, the sample was removed and cooled naturally in ambient air. A detailed description of the synthesis apparatus and parameters can be found elsewhere.[28,33] Water splitting three electrode voltammetry measurements were carried out in 1M NaOH aqueous solution using a PEC test cell (so-called the 'cappuccino cell', described in Reference [51]) with a platinum counter electrode and an Ag/AgCl reference electrode. The sample was illuminated from the front side using a solar simulator (ABET Sun 3000 class AAA solar simulator). The output radiation from the solar simulator was focused onto the photoanode using a Fresnel lens (Thorlabs FRP251), and the flux concentration was controlled by changing the distance between the photoanode and the lens, thereby ensuring that the normalized spectrum remains the same regardless of the degree of flux concentration. The illuminated area of the photoanode was 0.28 cm^2. More details on the flux concentration calibration are given in the supporting information (see Figure S8). In order to diminish spurious heating at high flux concentrations the radiation was chopped during measurements at flux concentrations above 3.6 for sample A and 2.6 for sample B. For sample A, the period of the chopping cycle was 15 s with a duty cycle of 20%. For sample B, the period of the chopping cycle was 16 s with a duty cycle of 25%. The maximum temperature rise during these measurements was found to be less than 10°C, as explained in the supporting information (see Figure S11). The applied potential was increased from 0.7 to 1.9 V vs. RHE for flux concentrations below 5.4. For flux concentrations above 5.4 the applied potential was increased from 0.7 to 2 V vs. RHE.

Supporting Information

Supporting Information is available from the Wiley Online Library or from the author.

[1]   N. S. Lewis, D. G. Nocera, *Proc. Natl. Acad. Sci. U. S. A.* **2006**, *103*, 15729.

[2]   J. Barber, P. D. Tran, *J. R. Soc. Interface* **2013**, *10*, 20120984.

[3]   M. Grätzel, *Nature* **2001**, *414*, 338.

[4]   M. G. Walter, E. L. Warren, J. R. McKone, S. W. Boettcher, Q. Mi, E. a Santori, N. S. Lewis, *Chem. Rev.* **2010**, *110*, 6446.

[5]   G. A. Olah, *Angew. Chem. Int. Ed. Engl.* **2005**, *44*, 2636.

[6]   W. Wang, S. Wang, X. Ma, J. Gong, *Chem. Soc. Rev.* **2011**, *40*, 3703.

[7]   K. Sivula, F. Le Formal, M. Grätzel, *ChemSusChem* **2011**, *4*, 432.

[8]   Y. Lin, G. Yuan, S. Sheehan, S. Zhou, D. Wang, *Energy Environ. Sci.* **2011**, *4*, 4862.

[9]   M. J. Katz, S. C. Riha, N. C. Jeong, A. B. F. Martinson, O. K. Farha, J. T. Hupp, *Coord. Chem. Rev.* **2012**, *256*, 2521.

[10] D. K. Bora, A. Braun, E. C. Constable, *Energy Environ. Sci.* **2013**, *6*, 407.

[11] K. M. H. Young, B. M. Klahr, O. Zandi, T. W. Hamann, *Catal. Sci. Technol.* **2013**, *3*, 1660.

[12] R. D. L. Smith, M. S. Prévot, R. D. Fagan, Z. Zhang, P. A. Sedach, M. K. J. Siu, S. Trudel, C. P. Berlinguette, *Science* **2013**, *340*, 60.

[13] M. S. Prévot, K. Sivula, *J. Phys. Chem. C* **2013**, *117*, 17879.

[14] F. J. Morin, *Phys. Rev.* **1954**, *93*, 1195.

[15] A. G. Joly, J. R. Williams, S. A. Chambers, G. Xiong, W. P. Hess, D. M. Laman, *J. Appl. Phys.* **2006**, *99*, 053521.

[16] D. L. Meier, J.-M. Hwang, R. B. Campbell, *IEEE Trans. Electron Devices* **1988**, *35*, 70.

[17] J. H. Kennedy, *J. Electrochem. Soc.* **1978**, *125*, 709.

[18] S. C. Warren, in Photoelectrochemical Hydrogen Production, (Eds: R. van de Krol, M. Grätzel), Wiley-VCH, Springer US, Boston, MA, 2012, Ch. 9.

[19] W. Gärtner, *Phys. Rev.* **1959**, *116*, 84.

[20] H. Dotan, K. Sivula, M. Grätzel, A. Rothschild, S. C. Warren, *Energy Environ. Sci.* **2011**, *4*, 958.

[21] M. Barroso, S. R. Pendlebury, A. J. Cowan, J. R. Durrant, *Chem. Sci.* **2013**, *4*, 2724.

[22] S. R. Pendlebury, M. Barroso, A. J. Cowan, K. Sivula, J. Tang, M. Grätzel, D. Klug, J. R. Durrant, *Chem. Commun.* **2011**, *47*, 716.

[23] S. R. Pendlebury, A. J. Cowan, M. Barroso, K. Sivula, J. Ye, M. Grätzel, D. R. Klug, J. Tang, J. R. Durrant, *Energy Environ. Sci.* **2012**, *5*, 6304.

[24] A. J. Cowan, J. R. Durrant, *Chem. Soc. Rev.* **2013**, *42*, 2281.

[25] L. M. Peter, *J. Solid State Electrochem.* **2012**, *17*, 315.

[26] F. Le Formal, S. R. Pendlebury, M. Cornuz, S. D. Tilley, M. Grätzel, J. R. Durrant, *J. Am. Chem. Soc.* **2014**, *136*, 2564.

[27] H. Dotan, O. Kfir, E. Sharlin, O. Blank, M. Gross, I. Dumchin, G. Ankonina, A. Rothschild, *Nat. Mater.* **2013**, *12*, 158.

[28] S. C. Warren, K. Voïtchovsky, H. Dotan, C. M. Leroy, M. Cornuz, F. Stellacci, C. Hébert, A. Rothschild, M. Grätzel, *Nat. Mater.* **2013**, *12*, 842.

[29] J. Y. Kim, G. Magesh, D. H. Youn, J.-W. Jang, J. Kubota, K. Domen, J. S. Lee, *Sci. Rep.* **2013**, *3*, 2681.

[30] T. Hisatomi, H. Dotan, M. Stefik, K. Sivula, A. Rothschild, M. Grätzel, N. Mathews, *Adv. Mater.* **2012**, *24*, 2699.

[31] M. Barroso, A. J. Cowan, S. R. Pendlebury, M. Grätzel, D. R. Klug, J. R. Durrant, *J. Am. Chem. Soc.* **2011**, *133*, 14868.

[32] C. Du, X. Yang, M. T. Mayer, H. Hoyt, J. Xie, G. McMahon, G. Bischoping, D. Wang, *Angew. Chem. Int. Ed. Engl.* **2013**, *52*, 12692.

[33] S. D. Tilley, M. Cornuz, K. Sivula, M. Grätzel, *Angew. Chem. Int. Ed. Engl.* **2010**, *49*, 6405.

[34] O. Khaselev and J. A. Turner, *Science* **1998**, 280,425

[35] H. Wang, T. Deutsch, J. A. Turner, *J. Electrochem. Soc.* **2008**, *155*, F91.

[36] B. M. Klahr, T. W. Hamann, *Appl. Phys. Lett.* **2011**, *99*, 063508.

[37] F. Williams, A. J. Nozik, *Nature* **1978**, *271*, 137.

[38] B. A. Gregg, A. J. Nozik, *J. Phys. Chem.* **1993**, *97*, 13441.

[39] P. Salvador, *J. Phys. Chem. B* **2001**, *105*, 6128.

[40] A. Kumar, P. G. Santangelo, N. S. Lewis, *J. Phys. Chem.* **1992**, *96*, 834.

[41] K. G. Upul Wijayantha, S. Saremi-Yarahmadi, L. M. Peter, *Phys. Chem. Chem. Phys.* **2011**, *13*, 5264.

[42] H. Dotan, N. Mathews, T. Hisatomi, M. Grätzel, A. Rothschild, *J. Phys. Chem. Lett.* **2014**, *5*, 3330.

[43] K. D. Malviya, H, Dotan, K.-R. Yoon, I.-D. Kim, A. Rothschild, *J. Mater. Res.* (submitted).

[44] D. Cao, W. Luo, J. Feng, X. Zhao, Z. Li, Z. Zou, *Energy Environ. Sci.* **2014**, *7*, 752.

[45] R. L. Doyle, I. J. Godwin, M. P. Brandon, M. E. G. Lyons, *Phys. Chem. Chem. Phys.* **2013**, *15*, 13737.

[46] W. Oelßner, F. Berthold, U. Guth, *Mater. Corros.* **2006**, *57*, 455.

[47] R. H. Coridan, A. C. Nielander, S. A. Francis, M. T. McDowell, V. Dix, S. M. Chatman, N. Lewis, *Energy Environ. Sci.* **2015**, DOI 10.1039/C5EE00777A.

[48] A. Cuevas, R. A. Sinton, N. E. Midkiff, R. M. Swanson, *IEEE Electron Device Lett.* **1990**, *11*, 6.

[49]   H. F. MacMillan, H. C. Hamaker, N. R. Kaminar, M. S. Kuryla, M. L. Ristow, D. D. Liu, G. F. Virshup, J. M. Gee, in *Conf. Rec. Twent. IEEE Photovolt. Spec. Conf.*, IEEE, **1988**, pp. 462–468.

[50]   J. S. Ward, K. Ramanathan, F. S. Hasoon, T. J. Coutts, J. Keane, M. A. Contreras, T. Moriarty, R. Noufi, *Prog. Photovoltaics Res. Appl.* **2002**, *10*, 41.

[51]   T. Lopes, L. Andrade, H. A. Ribeiro, A. Mendes, *Int. J. Hydrogen Energy* **2010**, *35*, 11601.